Supporting Information

Negative linear compressibility and structural stability of the energetic material *trans*-hexanitrostilbene under pressure

Xinglong Deng[a], Dong Li,[b] Boyang Fu[a], Yu Liu[a], Weilong He[a], Shourui Li[b*] and Weizhao Cai[a,c*]

[a] *School of Materials and Energy, University of Electronic Science and Technology of China, Chengdu 611731, Sichuan, China*

[b] *National Key Laboratory of Shock Wave and Detonation Physics, Institute of Fluid Physics, China Academy of Engineering Physics, Mianyang 621900, China*

[c] *Huzhou Key Laboratory of Smart and Clean Energy, Yangtze Delta Region Institute (Huzhou), University of Electronic Science and Technology of China, Huzhou 313001, Zhejiang, China*

Corresponding authors: lishourui1203@163.com; wzhcai@uestc.edu.cn

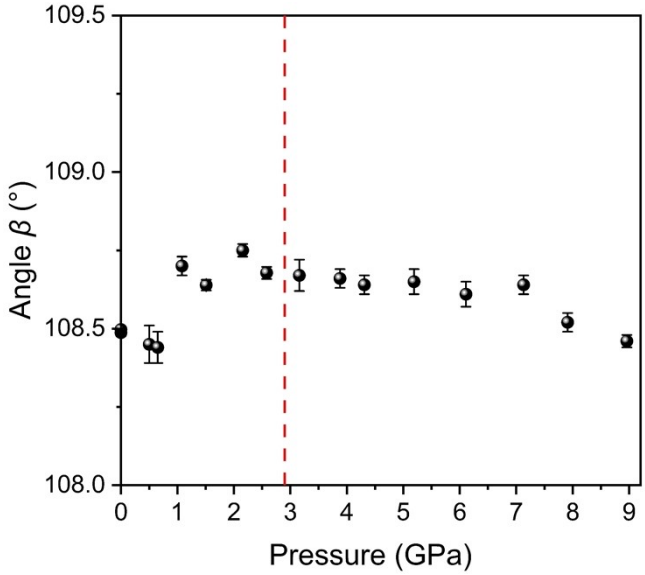

Figure S1. Unit-cell parameter angle β of *trans*-HNS as a function of pressure.

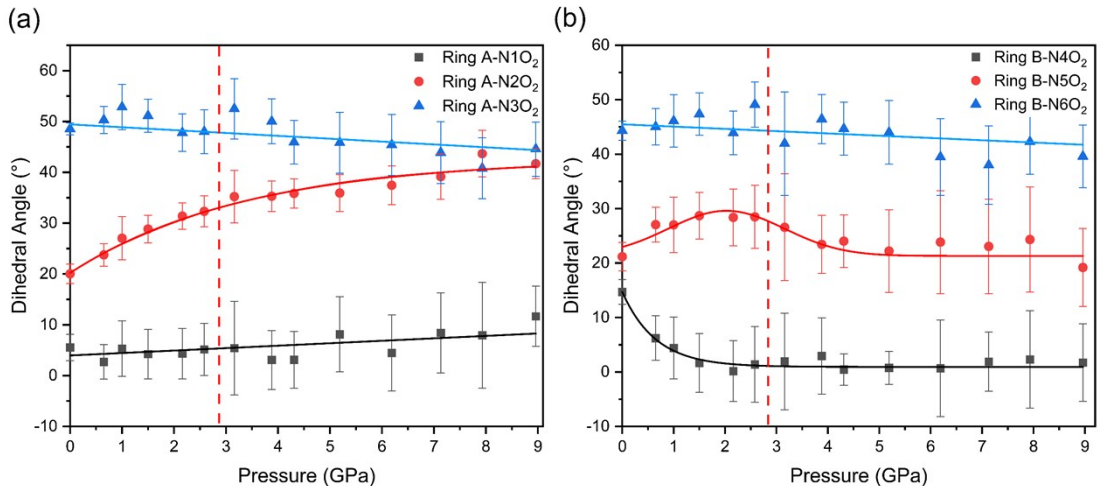

Figure S2. Dihedral angles between the nitro groups and (a) ring on Molecule A (Ring A) and (b) ring on Molecule B (Ring B) in the HNS molecule as a function of pressure.

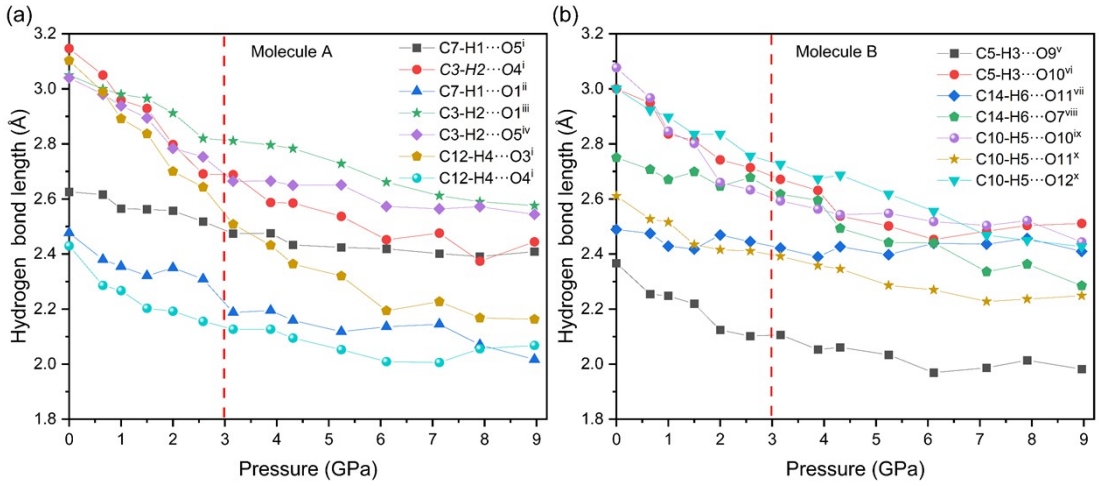

Figure S3. The variations of lengths of different C-H···O intermolecular contacts under pressure in Molecule A (a) and Molecule B (b). Lines are provided to guide the eye. Symmetry codes: (i) *x*, 1+*y*, *z*; (ii) 1-*x*, 2-*y*, 1-*z*; (iii) 1-*x*, -1/2+*y*, 1/2-*z*; (iv) *x*, 1/2-*y*, -1/2+*z*; (v) *x*, 1/2-*y*, 1/2+*z*; (vi) *x*, 1.5-*y*, 1/2+*z*; (vii) *x*, -1+*y*, *z*; (viii) -*x*, -*y*, -*z*; (ix) *x*, -1+*y*, *z*; (x) *x*, 1.5-*y*, -1/2+*z*.

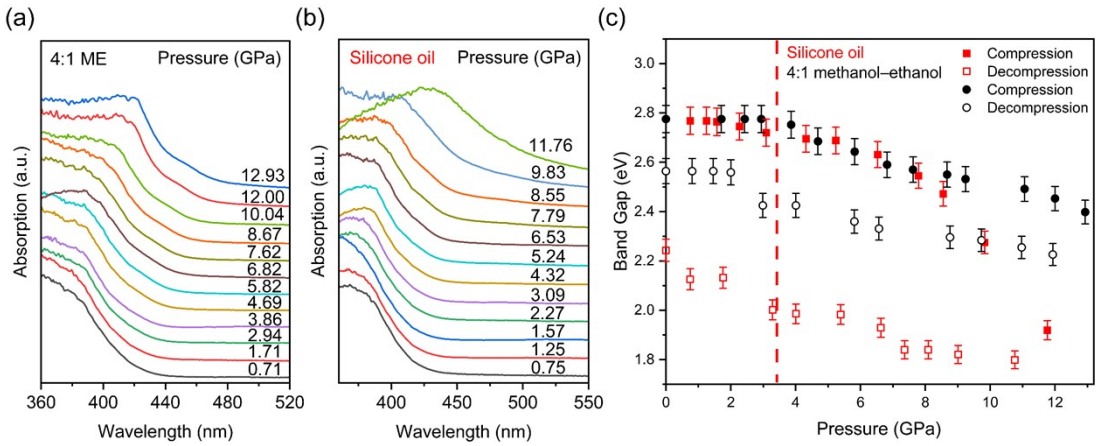

Figure S4. (a) Evolution of the absorption spectra using ME mixture as the PTM under pressure. (b) Pressure-dependent absorption spectra using silicone oil as the PTM. (c) Variations in the band gap of the sample during the compression-decompression process in ME and silicone oil.

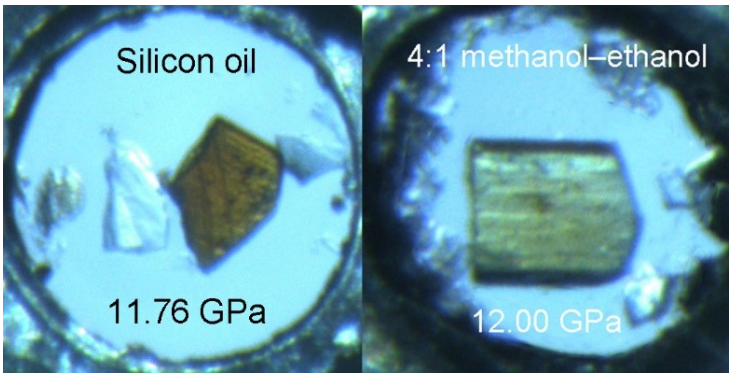

Figure S5. Comparison of the images of HNS single crystals compressed in silicone oil (at 11.76 GPa) and ME (at 12.00 GPa).

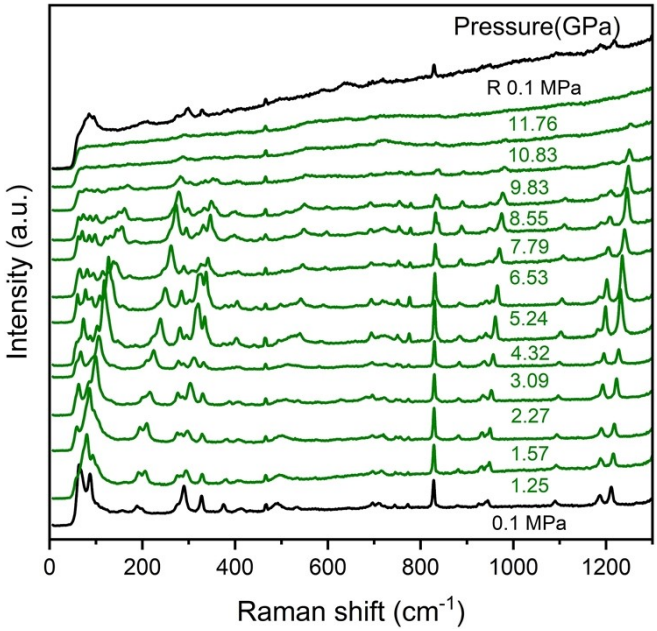

Figure S6. Selected Raman spectra of *trans*-HNS using silicone oil as the PTM in the range from 0 to 1300 cm^{-1} upon compression to 11.76 GPa. The black curve indicates the decompression data to 0.1 MPa.

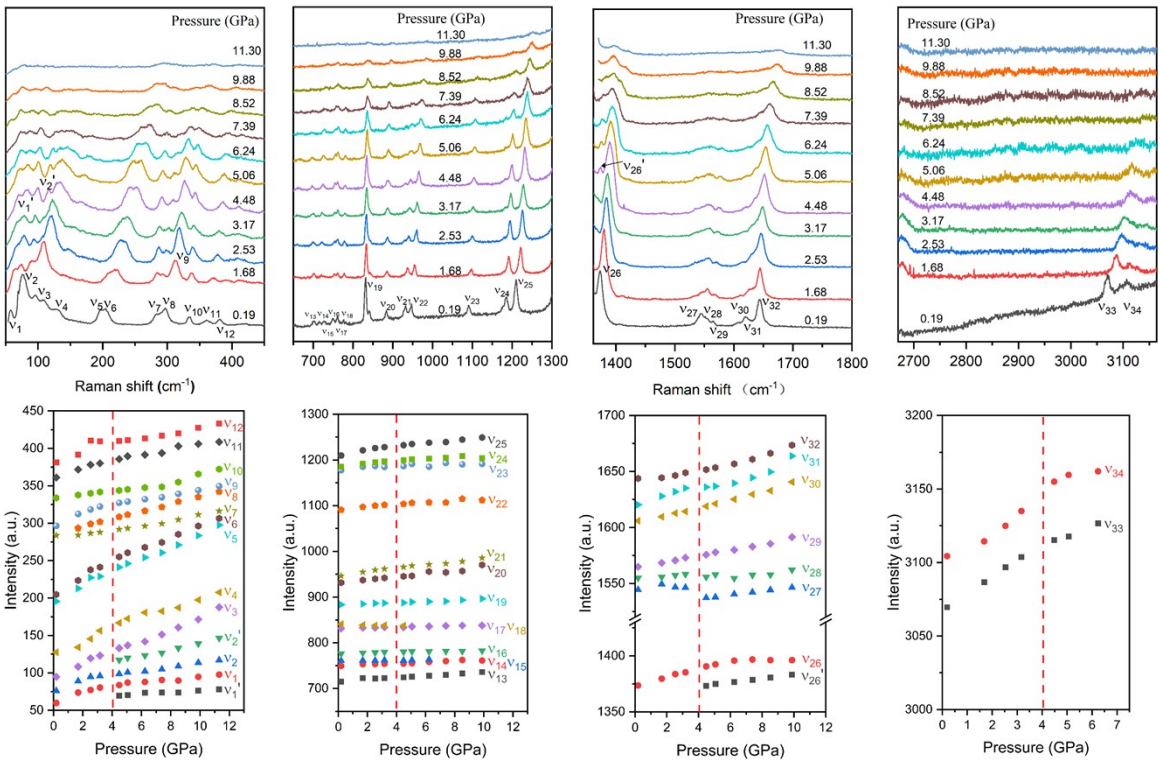

Figure S7. Selected Raman spectra of *trans*-HNS in the range from 50 cm^{-1} to 3200 cm^{-1} upon compression to 11.30 GPa using argon as the PTM. The evolutions of Raman modes during compression are demonstrated at the bottom.

Table S1. Selected crystallographic data of *trans*-HNS single crystal compressed in ME mixture at room temperature.

Pressure (GPa)	0.0001	0.60	1.00	1.52	2.16
CCDC	2394370	2394363	2394365	2394368	2394360
Crystal system	monoclinic	monoclinic	monoclinic	monoclinic	monoclinic
Space group	$P2_1/c$	$P2_1/c$	$P2_1/c$	$P2_1/c$	$P2_1/c$
Phase	I	I	I	I	I
Radiation type	MoKα	MoKα	MoKα	MoKα	MoKα
Crystal size (mm)	0.22 × 0.14× 0.05	0.21 × 0.14 × 0.05	0.21 × 0.14 × 0.05	0.21 × 0.14 × 0.05	0.21 × 0.14 × 0.05
a (Å)	22.122(2)	21.688(15)	21.434(12)	21.300(8)	21.024(10)
b (Å)	5.5747(4)	5.3559(13)	5.2569(8)	5.1648(5)	5.0460(6)
c (Å)	14.6672(13)	14.757(5)	14.764(3)	14.7908(16)	14.8201(19)
α (°)	90	90	90	90	90
β (°)	108.487(11)	108.44(5)	108.70(3)	108.639(17)	108.75(2)
γ (°)	90	90	90	90	90
V (Å^3)	1715.5(3)	1626.1(14)	1575.7(10)	1541.8(6)	1488.8(7)
Z	4	4	4	4	4
ρ_{calc}(g/cm^3)	1.743	1.839	1.898	1.940	2.009
μ(mm^{-1})	0.157	0.165	0.171	0.174	0.181
Index ranges	$-31 \le h \le 24$ $-7 \le k \le 7$ $-18 \le l \le 17$	$-10 \le h \le 11$ $-6 \le k \le 6$ $-13 \le l \le 13$	$-10 \le h \le 10$ $-6 \le k \le 6$ $-13 \le l \le 13$	$-9 \le h \le 9$ $-6 \le k \le 6$ $-13 \le l \le 13$	$-10 \le h \le 10$ $-6 \le k \le 6$ $-13 \le l \le 13$
R_{int}	0.0587	0.1242	0.1617	0.0765	0.0816
GOOF	1.022	1.133	1.222	1.089	1.140
R_1/wR_2 [I>2σ(I)][a]	0.0564/0.1335	0.0486/0.0903	0.0766/0.1801	0.0879/0.1986	0.1308/0.2890
R_1/wR_2 [all data]	0.1149/0.1559	0.1174/0.1213	0.1525/0.2668	0.1309/0.2436	0.1660/0.3270
Largest peak/hole (e·Å^{-3})	0.25/-0.29	0.09/-0.09	0.12/-0.11	0.15/-0.14	0.28/-0.28

Table S1 (continued)

Pressure (GPa)	2.59	3.16	3.88	4.31	5.19
CCDC	2394364	2394361	2394366	2394362	2394359
Crystal system	monoclinic	monoclinic	monoclinic	monoclinic	monoclinic
Space group	$P2_1/c$	$P2_1/c$	$P2_1/c$	$P2_1/c$	$P2_1/c$
Phase	I	I'	I'	I'	I'
Radiation type	MoKα	MoKα	MoKα	MoKα	MoKα
Crystal size (mm)	0.20 × 0.14 × 0.05	0.20 × 0.14 × 0.04	0.19 × 0.14 × 0.04	0.19 × 0.14 × 0.04	0.19 × 0.14× 0.04
a (Å)	20.995(8)	21.00(2)	20.771(12)	20.684(11)	20.526(16)
b (Å)	4.9882(5)	4.9406(14)	4.8819(8)	4.8371(7)	4.7810(10)
c (Å)	14.8276(17)	14.773(5)	14.771(3)	14.739(3)	14.686(3)
α (°)	90	90	90	90	90
β (°)	108.678(19)	108.67(5)	108.66(3)	108.64(3)	108.65(4)
γ (°)	90	90	90	90	90
V (Å^3)	1471.1(6)	1452.3(17)	1419.0(9)	1397.3(9)	1365.5(12)
Z	4	4	4	4	4
ρ_{calc}(g/cm^3)	2.033	2.059	2.107	2.140	2.190
μ(mm^{-1})	0.183	0.185	0.190	0.192	0.197
Index ranges	$-9 \le h \le 9$ $-6 \le k \le 6$ $-13 \le l \le 13$	$-9 \le h \le 9$ $-6 \le k \le 6$ $-13 \le l \le 13$	$-10 \le h \le 10$ $-6 \le k \le 6$ $-13 \le l \le 13$	$-9 \le h \le 9$ $-6 \le k \le 6$ $-13 \le l \le 13$	$-9 \le h \le 9$ $-6 \le k \le 6$ $-13 \le l \le 13$
R_{int}	0.0924	0.1504	0.0964	0.0769	0.1053
GOOF	1.188	1.208	1.071	1.070	1.106
R_1/wR_2 [$I>2\sigma$(I)][a]	0.1064/0.2301	0.0856/0.1897	0.0854/0.2032	0.0656/0.1671	0.0752/0.1825
R_1/wR_2 [all data]	0.1315/0.2596	0.1327/0.2542	0.1222/0.2389	0.0906/0.1944	0.1113/0.2112
Largest peak/hole (e·Å^{-3})	0.19/-0.16	0.16/-0.20	0.23/-0.23	0.15/-0.12	0.15/-0.15

Table S1 (continued)

Pressure (GPa)	6.11	7.13	7.91	8.95
CCDC	2394367	2394369	2394358	2394371
Crystal system	monoclinic	monoclinic	monoclinic	monoclinic
Space group	$P2_1/c$	$P2_1/c$	$P2_1/c$	$P2_1/c$
Phase	I'	I'	I'	I'
Radiation type	MoKα	MoKα	MoKα	MoKα
Crystal size (mm)	0.19 × 0.14 × 0.04	0.19 × 0.14 × 0.04	0.19 × 0.14 × 0.04	0.18 × 0.14 × 0.04
a (Å)	20.499(19)	20.416(13)	20.443(11)	20.421(10)
b (Å)	4.7253(10)	4.6742(8)	4.6447(6)	4.6057(6)
c (Å)	14.628(4)	14.559(3)	14.546(2)	14.4942(19)
α (°)	90	90	90	90
β (°)	108.61(4)	108.64(3)	108.52(3)	108.46(2)
γ (°)	90	90	90	90
V (Å^3)	1342.8(14)	1316.4(9)	1309.6(8)	1293.1(7)
Z	4	4	4	4
ρ_{calc}(g/cm^3)	2.227	2.272	2.284	2.313
μ(mm^{-1})	0.200	0.204	0.205	0.208
Index ranges	$-9 \le h \le 9$ $-6 \le k \le 6$ $-13 \le l \le 13$	$-9 \le h \le 9$ $-6 \le k \le 6$ $-13 \le l \le 13$	$-9 \le h \le 9$ $-5 \le k \le 5$ $-13 \le l \le 13$	$-9 \le h \le 9$ $-5 \le k \le 5$ $-13 \le l \le 13$
R_{int}	0.0938	0.0919	0.0907	0.1347
GOOF	1.106	1.078	1.047	1.045
R_1/wR_2 [$I>2\sigma$(I)][a]	0.0687/0.1619	0.0748/0.1478	0.0752/0.1802	0.0880/0.2123
R_1/wR_2 [all data]	0.0971/0.1847	0.1046/0.1689	0.0991/0.2049	0.1172/0.2430
Largest peak/hole (e·Å^{-3})	0.18/-0.19	0.13/-0.17	0.14/-0.16	0.18/-0.16

[a] $R_1 = \sum ||F_o|-|F_c|| / \sum |F_o|$ for $F_o^2 > 2\sigma(F_o^2)$; $wR_2 = \sum [w(F_o^2-F_c^2)] / \sum [w(F_o^2)^2]^{1/2}$, where $w = 1/[\sigma^2 F_o^2 + (A\,P)^2 + BP]$, and $P = (F_o^2 + 2F_c^2)/3$.

Table S2. Principal axes of the strain tensor and their mean linear compressibility coefficients of *trans*-HNS compressed in the ME mixture in phase I and phase I' (TPa^{-1}, $\times 10^{-3}$ GPa^{-1}).

Phase I (0-2.59 GPa)				
Eigenvalue		Crystal direction		
Axes	β_i (TPa^{-1})	*a*	*b*	*c*
X_1	41.6(3)	0	1	0
X_2	19.9(2)	0.9552	0	0.2961
X_3	-4.4(5)	0.0791	0	0.9969
V	55.0(7)			

Table S2. (continued)

Phase I' (3.16-8.95 GPa)				
Eigenvalue		Crystal direction		
Axes	β_i (TPa^{-1})	*a*	*b*	*c*
X_1	13.1(4)	0	1.0000	0
X_2	4.1(6)	0.9771	0	0.2127
X_3	3.5(5)	0.1226	0	0.9925
V	18.6(2)			

Table S3. Assignments of Raman spectra of *trans*-HNS single crystal.

Phase I 0.1 MPa	Raman shift (cm^{-1})	Assignments	Phase I' 8.62 GPa	Raman shift (cm^{-1})	Assignments
v_1		NO_2 torsion	v_1	75.52	NO_2 torsion
v_2		NO_2 torsion	v_2	92.30	NO_2 torsion
v_3		NO_2 torsion	v_3	105.95	NO_2 torsion
v_4		NO_2 torsion	v_4	127.37	NO_2 torsion
v_5		NO_2 torsion	v_5	139.91	NO_2 torsion
v_6	69.51	NO_2 torsion	v_6	153.85	NO_2 torsion
v_7	88.01	NO_2 torsion	v_7	166.16	NO_2 torsion
v_8	98.31	NO_2 torsion	v_8	197.38	NO_2 torsion
v_9	199.28	ring C-C out of plane bend	v_9	269.75	ring C-C out of plane bend
v_{10}	200.01	ring C-C out of plane bend	v_{10}	284.66	ring C-C out of plane bend
v_{11}	276.97	ring out of plane deformation	v_{11}	300.10	ring out of plane deformation
v_{12}	288.97	NO_2 in plane rock, ring twist	v_{12}	338.88.	NO_2 in plane rock, ring twist
v_{12}'		NO_2 in plane rock, ring twist	v_{12}'	324.92	NO_2 in plane rock, ring twist
v_{13}	328.88	C-N in plane rock, ring in plane bend	v_{13}	351.49	C-N in plane rock, ring in plane bend
v_{14}	753.67	NO_2 out of plane bend, ring torsion	v_{14}	756.24	NO_2 out of plane bend, ring torsion
v_{15}	772.12	ring in plane bend, C-C=stretching	v_{15}	780.52	ring in plane bend, C-C=stretching
v_{16}	829.34	sci (NO_2)	v_{16}	833.86	sci (NO_2)
v_{16}'		sci (NO_2)	v_{16}'	839.21	sci (NO_2)
v_{17}	880.79	sci (NO_2), ring in plane bend	v_{17}	892.12	sci (NO_2), ring in plane bend
v_{18}	929.13	C-N stretching	v_{18}	953.88	C-N stretching
v_{19}	944.01	HC=CH wag	v_{19}	982.81	HC=CH wag
v_{20}	1091.37	C-H (in ring) in plane bend, ring breath	v_{20}	1113.64	C-H (in ring) in plane bend, ring breath
v_{21}	1173.65	C-C (ring) in plane bend	v_{21}	1192.96	C-C (ring) in plane bend
v_{22}	1187.38	C-C (ring) in plane bend	v_{22}	1210.96	C-C (ring) in plane bend
v_{23}	1212.09	ring breath	v_{23}	1252.71	ring breath
v_{24}	1337.42	$v_s(NO_2)$[a]	v_{24}	1397.48	$v_s(NO_2)$
v_{24}'		$v_s(NO_2)$	v_{24}'	1384.81	$v_s(NO_2)$
v_{24}''		$v_s(NO_2)$	v_{24}''	1434.35	$v_s(NO_2)$
v_{25}	1537.46	v_{as} (NO_2)[b]	v_{25}	1538.87	v_{as} (NO_2)
v_{25}'		v_{as} (NO_2)	v_{25}'	1549.04	v_{as} (NO_2)
v_{26}	1550.21	v_{as} (NO_2)	v_{26}	1568.40	v_{as} (NO_2)
v_{27}	1562.99	v_{as} (NO_2)	v_{27}	1585.06	v_{as} (NO_2)
v_{28}	1605.21	v(C=C) in aromatic ring	v_{28}	1630.42	v(C=C) in aromatic ring
v_{29}	1618.89	v(C=C) in aromatic ring, ring stretching	v_{29}	1649.14	v(C=C) in aromatic ring, ring stretching
v_{30}	1642.93	v(C=C) in –CH=CH–	v_{30}	1666.85	v(C=C) in –CH=CH–
v_{31}	2907.30		v_{31}	2907.30	
v_{32}	2965.93		v_{32}	2965.93	
v_{33}	3064.69	v(C-H) in –CH=CH–	v_{33}	3143.14	v(C-H) in –CH=CH–
v_{33}'			v_{33}'	3161.25	v(C-H) in –CH=CH–

[a] v_s (NO_2) means the symmetric stretching of NO_2; [b] v_{as} (NO_2) means the asymmetric stretching of NO_2